Citrated porous gel copolymer electrolyte composite for lithium ion batteries application: An investigation of ionic conduction in an optimized crystalline and porous structure

Emad M. Masoud

Chemistry Department, Faculty of Science, Benha University, 13518 Benha, Egypt

ABSTRACT

Citrated porous PVDF-co-HFP containing $LiClO_4$–EC–DEC is prepared with a preferential polymer dissolution process using polyvinyl acetate to create a different porosity ratio of the optimized citrated membrane. All citrated samples (3,5,7,9,11 wt. %) are characterized using X-ray diffraction to show that the sample containing 7 wt. % citric acid has the lowest crystalline structure. The optimized sample is mixed with different PVA concentrations, (4, 8, 12, 16 wt. %), and then all PVA removal copolymer composite samples are immersed in a mixture of a liquid electrolyte containing $LiClO_4$, EC, and DEC. The swelling and porosity measurements show that the sample containing 16 wt. % of PVA removal has the highest values, 68% porosity and 115% swelling. Scanning electron microscope is used to show the porous structure of the optimized citrated copolymer electrolyte sample (16 wt. % of PVA removal) compared to the before removing PVA one. DC-electrical conductivity measurement is performed to show the effect of porosity on the conduction process. The sample having 8 wt. % PVA removal shows a high conductivity value of 8×10^{-4} S cm^{-1} compared to the other samples at room temperature. Complex impedance, electrochemical stability and stress–strain curve are also studied. All results are collected and discussed.

© 2015 Elsevier B.V. All rights reserved.

1. Introduction

In recent years, there has been a growing demand for high-energy density rechargeable lithium batteries for portable electronic products because of their advantages including safety, high-energy density, high single cell voltage, geometry and no memory effect. Polymer electrolytes, new electrolytic materials competing for a place in the future energy generation, storage and distribution markets. Polymer electrolytes offer many advantages over their more conventional liquid counterparts in these developing technologies, such as:flexibility, easy of processing into thin films of a large surface area, good mechanical stability, chemical - electrochemical stability and volumetric stability through charging and dis-charging processes. However, the ionic conductivity of polymer electrolytes is generally low, often too low for practical application. To improve the basic requirements of the polymer electrolyte, various processes have been used such as electrochemical stability towards lithium battery electrodes, compatibility with the

electrode materials, reasonable ionic conductivity, sufficient thermal stability and good mechanical stability.

Many polymers, such as polyethylene oxide (PEO) [1], polyacrylonitrile (PAN) [2], polymethylmethacrylate (PMMA) [3], and polyvinylidene fluoride (PVDF) [4–6], have been used too as matrices for polymer electrolytes. PVDF-HFP has been attracted as a highly promising material for the polymer electrolyte of rechargeable lithium battery because its high solubility and lower crystallinity and glass transition temperature than PVDF [7–11]. Moreover, it is a semi-crystalline polymer, in which the amorphous domains can trap more liquid electrolyte, and crystalline regions contribute to the improvement mechanical integrity while being processed in free-standing films.

Studies have been made primarily on the enhancement of the ionic conductivity at room temperature via various approaches such as blends, co-polymers, comb shape polymers, cross-linked networks and incorporation of ceramic fillers onto the polymer matrix. Organic acid such as citric acid is one of the important methods used to improve the ionic conductivity [12] in polymer electrolytes due to its strong ligating power to the lithium ion [13]. Also, the porous texture has proved an effective approach to

improve the overall performances of polymer electrolyte, which usually showed good mechanical performances with enhanced ionic conductivity at room temperature besides the activation process requires a critical moisture control only during the last activation step because of high water sensitivity of lithium salt [14–18].

In the present work, we try to prepare citrated gel copolymer electrolyte composites (citric acid + PVDF-co-HFP–LiClO₄-EC-DEC) with a porous structure to enhance the ionic motion within the copolymer matrix. The ionic motion in general will depend on the crystallinity and porosity ratios of the matrix. But the question is still what the optimum ratios of crystallinity and porosity are in a composite system to show an optimized structure with an optimum ionic motion, to get finally a good polymer electrolyte. Here, we used polyvinyl acetate to prepare different porosity ratios of PVDF-co-HFP electrolyte composites containing citric acid to study the porosity dependence of the conduction process.

2. Experimental

2.1. Materials

PVDF-co-HFP (M.wt = 550,000, Sigma–Aldrich), PVA (Sigma–Aldrich), Citric acid (Merck), LiClO₄ (Sigma–Aldrich), Ethylene carbonate (EC) and diethyl carbonate (DEC) (Sigma–Aldrich) were used as starting materials to prepare citric co-polymer composites and porous citric gel co-polymer electrolyte composites.

2.2. Preparation of citric co-polymer composites films

First, the co-polymer (PVDF-co-HFP) was dissolved in acetone. Different wt. % of citric acid (0, 3, 5, 7, 9 and 11 wt. %) were added. The resultant homogeneous viscous solutions were spread as films on a glass substrate. Then, the polymer composites films were dried at 50 °C in a vacuum oven for 6 h to remove any further traces of acetone. The thickness of the films was obtained in the range of 2–4 mm. Finally, the resultant citric polymer composites films were characterized using X-ray diffraction to optimize the citric acid content within PVDF-co-HFP matrix.

2.3. Preparation of porous citric gel co-polymer composites electrolytes films

The optimized sample of citric co-polymer composite was taken and dissolved in DMF. Polyvinyl acetate with different amounts (0, 4, 8, 12 and 16 wt. %) was also added. The resultant viscous solutions were spread as films on a glass substrate. These films were dried at 80 °C in a vacuum oven for 6 h to remove any further traces of DMF. The thickness of the films was determined to be in a range of 2–4 mm. The films were immersed in a pool of excess of deionized water at 60 °C to remove PVA from PVdF-co-HFP matrix to form a porous structure with different distribution ratios. These porous citric co - polymer composites membranes were dried under vacuum at 80 °C for 6 h. Finally, the samples were activated by soaking in 1 M LiClO₄ electrolyte solution containing 1:1 (v/v) ratio of EC and DEC (the electrolyte solution has a conductivity value of 8.5×10^{-3} S cm^{-1}) for 18 h to get porous citric gel co-polymer composites electrolytes.

2.4. Characterization of samples

X-ray diffraction analysis was performed on a Diano (made by Diano Corporation, U.S.A.) with Cu-filtered CuKα radiation (λ = 1.5418 Å) energized at 45 kV, and 10 mA. The samples were measured at room temperature in the range from 2θ = 10° to 70°.

Scanning electron microscope was carried out with JOEL-scanning electron microscope (JSM-35CF) to show the ability of PVA to create a porous structure within the matrix of the citric co-polymer composites.

The porosity (P) was determined using the following equation [9]:

$$P = \left[(m_a/\rho_a) \div (m_a/\rho_a + m_p/\rho_p) \right] \times 100 \qquad (1)$$

Where m_a is the weight of citric co-polymer composites after impregnation with 1-butanol and m_p is the weight of citric co-polymer composites before impregnation with 1-butanol. Similarly, ρ_a and ρ_p are density of 1-butanol and the citric co-polymer composites, respectively. Swelling behavior of the citric co-polymer composites was also studied. The extent of swelling (S_w) of citric co-polymer composites was determined to investigate its dependence on the porous structure. The percentage of swelling was determined using Eq. (2) [19]:

$$S_w = \left[(W - W_0) \div (W_0) \right] \times 100 \qquad (2)$$

Where W_0 is the weight of dried films and W is the weight of swelled films.

Differential thermal analysis (DTA) and thermal gravimetric analysis (TGA) were performed in Argon atmosphere with a constant heating rate of 10 K/min. in a temperature range of 298–473 K using Shimadzu DT-50.

The stress–strain characteristic was recorded at room temperature by using Bruker–Digital force gauge (1000 N). The sample was cast in a dimension of 60 mm × 20 mm. The thickness of cast sample is 2 mm.

2.5. Electrochemical characterization

The ionic conductivity measurements were performed by sandwiching the citric co-polymer electrolyte composites between two stainless steel electrodes using a programmable automatic LCR bridge (Model RM 6306 Phillips Bridge) in various temperatures ranging from 303 to 353 K. The electrochemical stability of citric co - polymer electrolyte composite having the highest ionic conductivity was evaluated with cell featuring a stainless steel (SS) as a working electrode and lithium as counter and reference electrodes by linear sweep voltammetry at 25 °C using an EG&G Electrochemical analyzer (Model-6310) in the scan rate of 1 mV/s. The cell was assembled in a glove box under argon atmosphere.

3. Results and discussion

3.1. Optimization of citric co-polymer composites

X-ray diffraction patterns of co-polymer with different wt. % of citric acid (0, 3, 5, 7, 9 and 11 wt. %) are displayed in Fig. 1. The figure showed an absence of citric acid crystalline peaks with the co-polymer at all concentrations and this may be attributed to the interaction of the polymer backbone and citric acid. Also, the figure showed that the sample containing 7 wt. % citric acid has low relative intensity peaks (low crystalline structure) and more broadening ones. This shows that the optimized concentration of citric acid within the PVDF-co-HFP matrix can be achieved when 7 wt. % is added. The values of crystallinity percent (X_c) were calculated from the intensity ratio of the peaks and tabulated in Table 1. The composite containing 7 wt. % citric acid showed lower X_c value (75%) than the other ones.
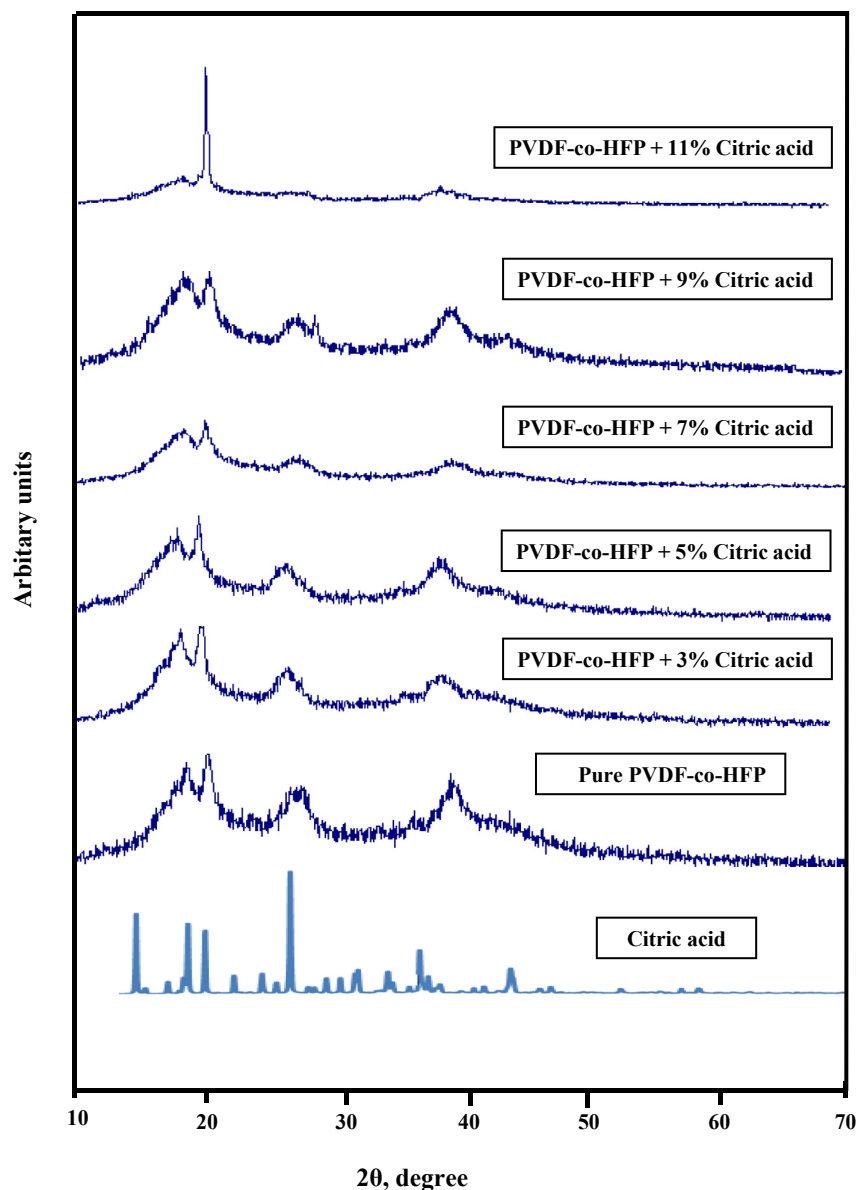
Fig. 1. XRD of citric acid, pure and composites of PVDF-co-HFP with different concentrations (wt.%) of citric acid.

3.2. Porosity, swelling behaviors and SEM

The porosity of the optimized co-polymer composite was calculated using Eq. (1). The porosity behavior is shown in Fig. 2. From this figure, it is observed that the removal of PVA content in the optimized co-polymer composite matrix creates the porous polymer membrane. The increase in removal of PVA content causes an increase in porosity. Hence, the uptake of electrolyte solution by the optimized co-polymer composite also increases with the increase in removal of PVA content as shown in Fig. 3. All values of porosity and swelling of the composites are tabulated in Table 2. To show the effect of PVA in creating a porous structure, the SEM photographs were taken for the optimized composition of PVDF- co -HFP– citric acid after and before a removal of 16 wt.% of PVA content (Fig. 4(A) and (B)). It can be seen from Fig. 4(A) that the before removal of PVA content in the co-polymer electrolyte matrix, could not observe a porous texture. The other one obtained by the removal of 16 wt. % of PVA in the co-polymer electrolyte matrix shows a porous structure, Fig. 4(B).

3.3. Optimization of co-polymer electrolytes composites films

All optimized co-polymer electrolytes composites were characterized using x-ray diffraction to show the interaction between the polymer matrix and liquid electrolyte. The X-ray diffraction figures are shown in Fig. 5(a)–(e) as a function of the removal of
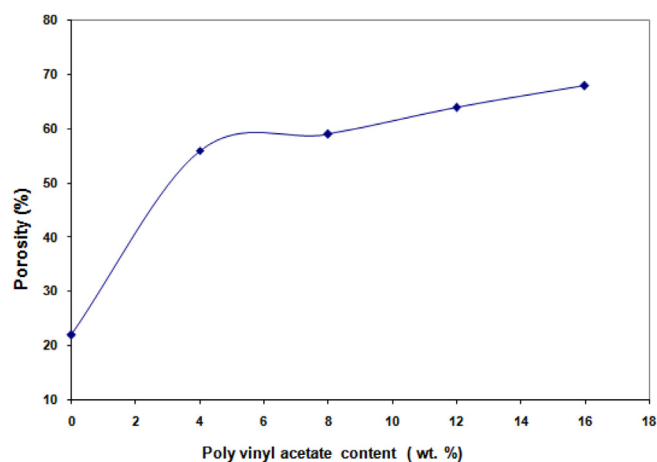
Table 1
Values of crystallinity (X$_c$) for citrated copolymer and citrated copolymer electrolytes composites.

Citrated copolymer composites, wt. % of citric acid	X$_c$ (%)	Citrated copolymer electrolytes composites, wt. % of PVA removal	X$_c$ (%)
0	90	0	80
3	84	4	76
5	80	8	68
7	75	12	78
9	78	16	95

Fig. 2. Porosity of optimized co-polymer composite against different polyvinyl acetate content.
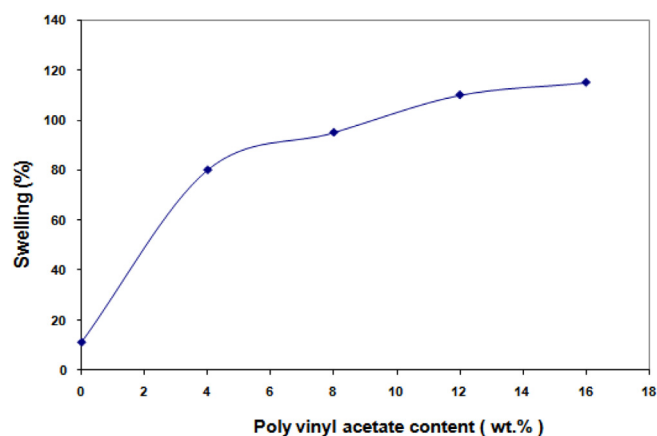
Fig. 3. Swelling of optimized co-polymer composite against different polyvinyl acetate content.

Fig. 4. SEM photographs for optimized copolymer electrolyte composite titled as: (A): before removing 16 wt. % PVA, (B): after removing 16 wt. % PVA.

Table 2
Values of porosity, swelling and activation energy (E_a) for optimized copolymer electrolytes composites.

Sample (wt. % PVA)	Porosity, %	Swelling, %	E_a (eV)
0	22	11	0.096
4	56	80	0.092
8	59	95	0.075
12	64	110	0.083
16	68	115	0.088

PVA content. The figures showed that all compositions (except C, C′) have obvious crystalline peaks characterized to LiClO₄ [20]. This shows that LiClO₄ has a good dissolution with composition C matrix (8 wt. % of PVA removal, 59% porosity) compared to the other ones. The crystalline percent values (Xc, %) were also calculated from the peak intensity ratios, Table 1. The table showed that the composition C has the lowest crystalline value (X_c = 68%), and this also shows the suitable structure of C composition for the liquid electrolyte interaction. The composition C was compared with a free liquid electrolyte composition (C′, Fig. 5). The absence of the electrolyte peaks in composition C to be like C′ confirmed a good interaction between the polymer matrix backbone and the liquid electrolyte.
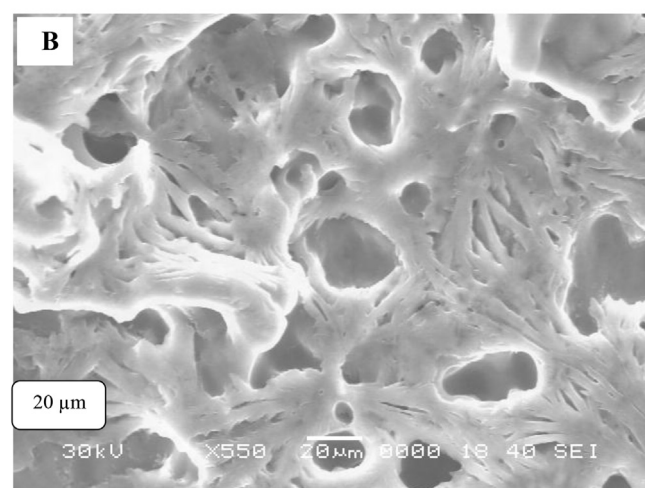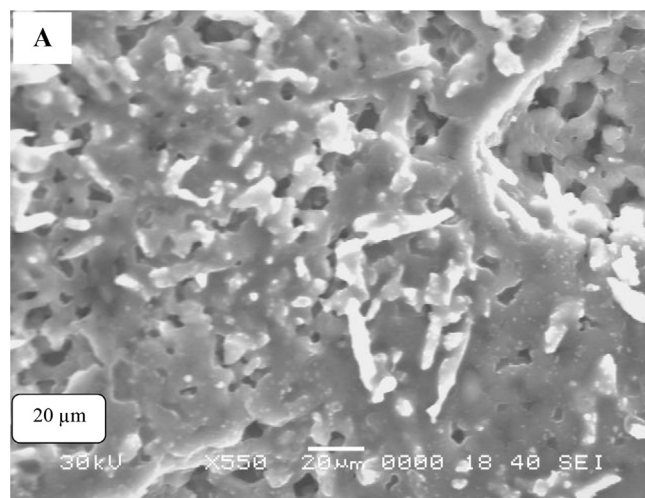
3.4. Optimization of lithium ion motion within the copolymer matrix

Fig. 6 displays Arrhenius plots of DC- conductivity of the copolymer electrolytes composites as a function of different wt. % of PVA content removal at different temperatures. It is noted that the ionic conductivity did not exhibit a same in tendency of porosity and the liquid electrolyte uptake shown in Figs. 2 and 3. The figure showed a maximum DC- ionic conductivity for the sample of 8 wt. % of PVA removal ($\sigma_{dc} = 8 \times 10^{-4}$ Scm^{-1} at room temperature). This comes in agreement with what observed from X-ray analysis where the same sample has the lowest crystalline percent (X_c) value (see Table 1).

The figure also shows that the DC-ionic conductivity of copolymer electrolytes composites increases in general with increase in temperature. Also, These curves appear linear, so the apparent activation energy for the ions transport (E_a) are obtained using the Arrhenius model $\sigma = \sigma_0 \exp(-E_a/RT)$, where R, T, σ and σ_0 are gas constant, temperature, the DC-ionic conductivity and the pre-exponential factor, respectively. According to this equation, the activation energy for the ions transport can be calculated from the slope of imitated straight line and are given in Table 2. From this table, it can be seen that the activation energy decreases with the removal of PVA content to have a minimum value of 0.075 eV for
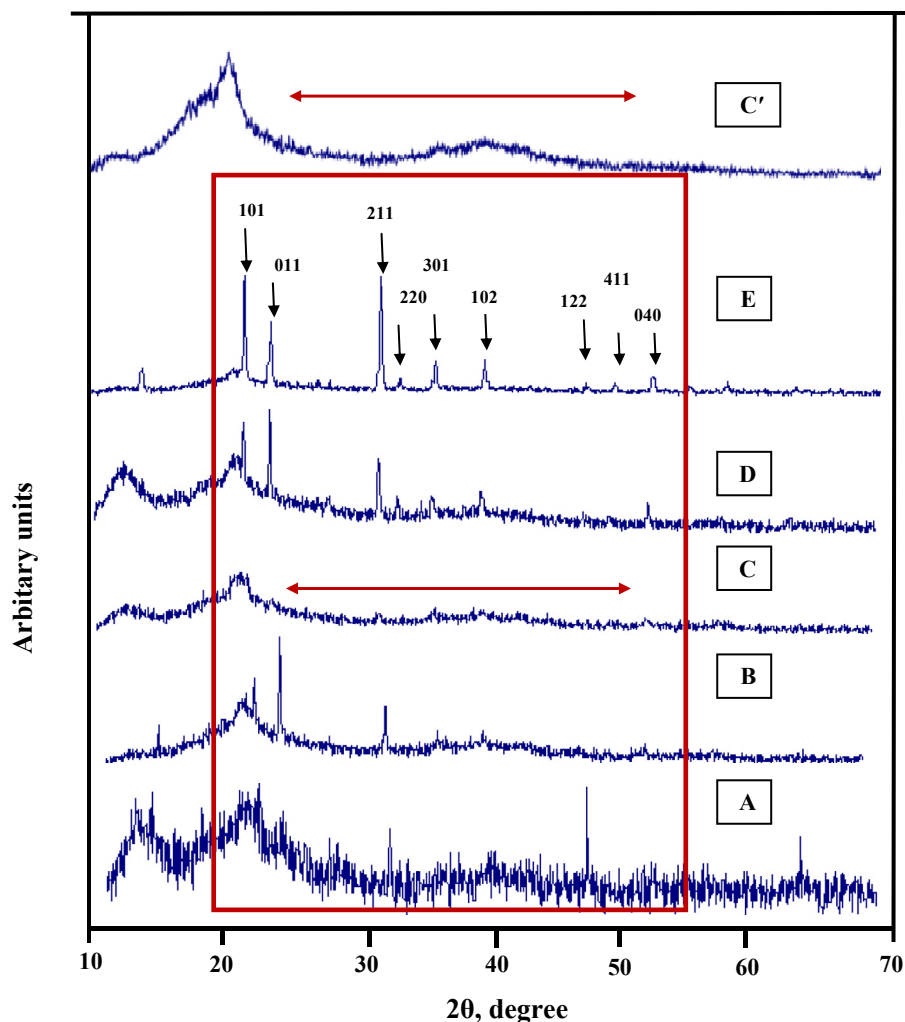
Fig. 5. XRD of co-polymer electrolytes composites as a function of removal of different wt. % of PVA: (A) 0 wt. %, (B) 4 wt. %, (C) 8 wt. %, (D) 12 wt. %, (E) 16 wt. %, C': co-polymer composite with 8 wt. % PVA removal.

the sample containing a removal of 8 wt. % PVA ($\sigma_{dc} = 8 \times 10^{-4}$ Scm^{-1} at room temperature), and returns again to increase. This can also show that the variation in porosity percent can influence the activation energy for ionic conduction.

The values variation of DC-ionic conductivity at room temperature with the porosity percent (PVA wt. % removal) were also

Fig. 6. Arrhenius plots of co-polymer electrolytes composites as a function of removal of different wt. % of PVA.

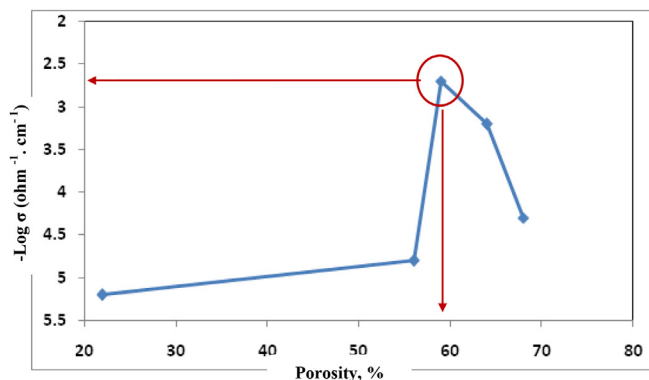shown in Fig. 7. The figure showed that the DC-ionic conductivity at room temperature has the following order: σ_{dc} (Porosity = 59%) > σ_{dc} (porosity = 68%) > σ_{dc} (porosity = 64%) > σ_{dc} (porosity = 56%) > σ_{dc} (porosity = 22%).

3.5. Thermal analysis of the optimized co-polymer electrolyte composite

Fig. 8, TGA of 8 wt. % PVA removal sample shows an almost stable weight till 80 °C. After that, a sharp decrease of weight was observed due to the thermal decomposition. Also, DTA shows an endothermic peak at around 150 °C that is characteristic to the melting temperature (T$_m$) of the sample.

3.6. Electrochemical stability

One of the important parameters in the characterization of optimized co-polymer electrolyte composite is the electrochemical stability window. This parameter can be determined by means of a linear sweep voltammetry (LSV). The resulting voltammogram for SS/OCEC/Li cell is shown in Fig. 9. The onset voltage for anodic current is determined at around 4.2 V versus Li/Li$^+$ which is assumed to be the decomposition voltage of the optimized sample.
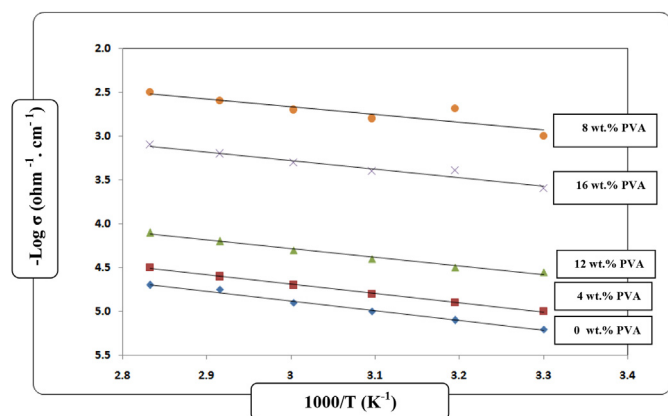
Fig. 7. Porosity dependence of dc-conductivity for co-polymer electrolytes composites at room temperature.

Fig. 8. DTA and TGA for optimized co-polymer electrolyte composite containing removal of 8 wt. % PVA.

3.7. Complex impedance

Fig. 10 shows a complex impedance plot of the optimized sample. The figure showed an impedance spectrum consists of a semi − circle and an inclined straight line. The semicircle is related to the conduction process and the linear region is due to the effect of the blocking electrode [21] that results in a charge polarization in the bulk of the copolymer, and as a result, the electrical double layer at each interface will lead to increase the impedance against ion motion with decreasing frequency. Also, the value of bulk ionic conductivity was calculated to equal 11×10^{-4} Scm^{-1} at room temperature. The equivalent circuit is also determined from the complex impedance spectrum and shown in Fig. 10. Where R_1 is the bulk resistance of the electrolyte, C_1 is the bulk capacity of the electrolyte and C_2 is a capacity of bulk electrode − electrolyte interface.

3.8. Stress−strain characteristic

The stress−strain curve of the optimized sample was also investigated, Fig. 11. The figure showed yield strength of 2.5 Mpa with an elongation −at− break of 15%. Also, the energy per unit volume i.e. toughness is 0.32 J.

4. Conclusions

A porous citrated gel copolymer electrolyte composite was prepared. With 7 wt. % citric acid and 8 wt.% PVA removal, the

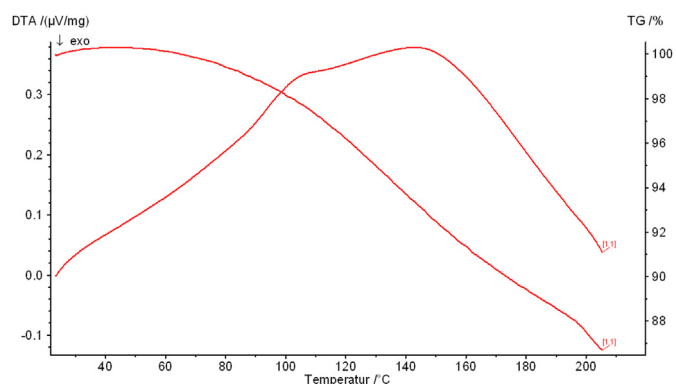**Fig. 9.** Linear sweep voltammetry curve of optimized co-polymer electrolyte composite containing removal of 8 wt. % PVA.

composite showed an optimized structure for the Li-ion conductivity. The crystalline percent of optimized citrated copolymer composite was calculated from the intensity ratio of x-ray diffraction peaks to equal 75%. Also, the crystalline and porosity percent of optimized citrated copolymer electrolyte composite were calculated by the same way to equal 68% and 59%, respectively.
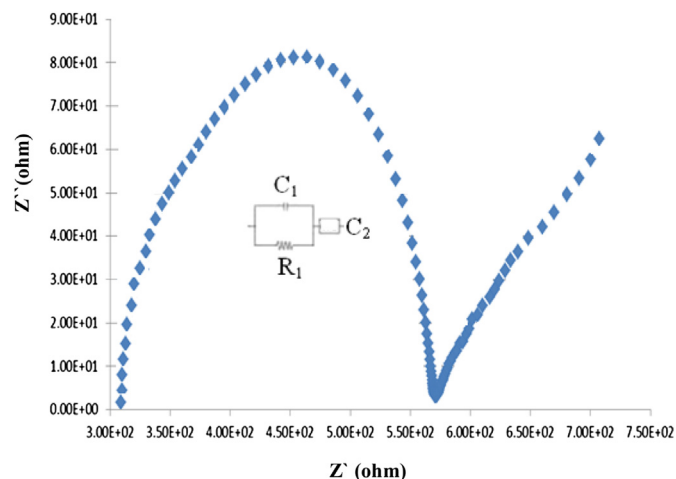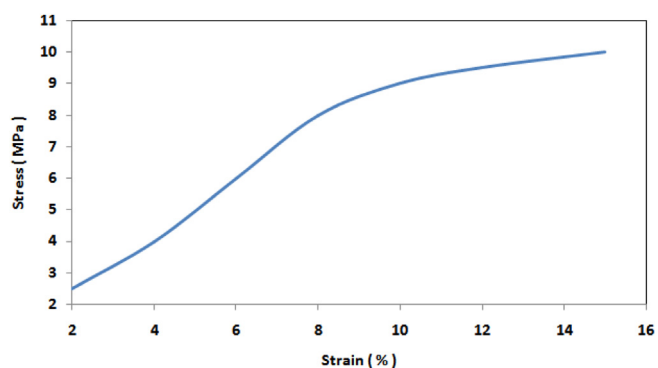

Fig. 10. Complex impedance of optimized co-polymer composite electrolyte containing removal of 8 wt. % PVA at room temperature.

Fig. 11. Stress−strain plot of optimized co-polymer composite electrolyte containing removal of 8 wt. % PVA at room temperature.

The porosity dependence of dc-ionic conductivity for the copolymer electrolytes composites at room temperature comes with the following order: σ_{dc}(Porosity = 59%) > σ_{dc} (porosity = 68%) > σ_{dc}(porosity = 64%) > σ_{dc} (porosity = 56%) > σ_{dc} (porosity = 22%). The DTA analysis showed that T_m of the optimized copolymer electrolyte composite is 150 °C. The onset voltage for anodic current is determined at around 4.2 V versus Li/Li$^+$ which is assumed to be the decomposition voltage of the optimized copolymer electrolyte composite. Also, the complex impedance showed a bulk conductivity of 11×10^{-4} Scm^{-1} and the equivalent circuit was determined. The mechanical test (stress–strain curve) of the optimized copolymer electrolyte composite showed yield strength of 2.5 Mpa with an elongation - at - break of 15%. This optimized copolymer electrolyte composite has a good conductivity at room temperature, making it a promising material for the lithium ion batteries application.

Acknowledgments

References

[1] E.M. Masoud, A.-A. El-Bellihi, W.A. Bayoumy, M.A. Mousa, Mater. Res. Bull. 3 (2013), 1148.
[2] H.K. Yoon, W.S. Chung, N.J. Jo, Electrochim. Acta 50 (2004) 289.
[3] G.B. Appetecchi, F. Croce, B. Scrosati, Electrochim. Acta 40 (1995) 991.
[4] E. Tsuchida, H. Ohno, K. Tsunemi, Electrochim. Acta 28 (1983) 591.
[5] H.P. Wang, H.T. Huang, L.W. Stephanie, J. Electrochem. Soc. 147 (2000) 2853.
[6] Z. Jiang, B. Carroll, K.M. Abraham, Electrochim. Acta 42 (1997) 2667.
[7] X. Zhou, L. Yue, J. Zhang, Q. Kong, Z. Liu, J. Yao, G. Cui, J. Elecrochem. Soc. 160 (2013) A1341.
[8] C. Lee, J.H. Kim, J.Y. Bae, Polymer 44 (2003) 7143.
[9] Q. Shi, M.X. Yu, X. Zhou, Y.S. Yan, C.R. Wan, J. Power Sources 103 (2002) 286.
[10] D. Saikia, A. Kumar, Electrochim. Acta 49 (2004) 2541.
[11] T. Michot, A. Nishimoto, M. Watanabe, Electrochim. Acta 45 (2000) 1347.
[12] I. Honma, S. Hirakawa, K. Yamada, J.M. Bae, Solid State Ion. 118 (1999) 29.
[13] J. Won Park, E. Duck Jeong, M. Sook Won, Y. Bo Shima, J. Power Sources 160 (2006) 674–680.
[14] H.S. Min, J.M. Ko, D.W. Kim, J. Power Sources 119 (2003) 469.
[15] J.D. Jeon, B.W. Cho, S.Y. Kwak, J. Power Sources 143 (2005) 219.
[16] S.S. Zhang, M.H. Ervin, K. Xu, T.R. Jow, Solid State Ion. 176 (2005) 41.
[17] A. Subramania, N.T. Kalyana Sundaram, N. Sukumar, J. Power Sources 141 (2005) 188.
[18] A. Subramania, N.T. Kalyana Sundaram, A. Rohini Priya, R. Gangadharan, T. Vasudevan, J. Appl. Polym. Sci. 98 (2005) 1891.
[19] T.C. Wen, H.H. Kuo, A. Gopalan, Solid State Ion. 147 (2002) 171.
[20] JSCPDS 96-431-393.
[21] Emad M. Masoud, A.-A. Elbellihi, W.A. Bayoumy, M.A. Mousa, Alloys Compd. 575 (2013), 223.